

Benchmarking of a fully-coupled three-dimensional low-temperature plasma and reactive Navier-Stokes solver

Alfredo Duarte Gomez*, Fabrizio Bisetti[†] *The University of Texas at Austin, Austin, Texas, 78712*

Nicholas Deak [‡],Lucas Esclapez[§], Marcus Day [¶] *The National Renewable Energy Laboratory, Golden, Colorado, 80401*

The three-dimensional exascale reactive solver PeleC with Adaptive Mesh Refinement (AMR) capabilities is extended to simulate low-temperature plasma streamer discharges. Charged species fluxes are modeled using the drift-diffusion approximation, which is incorporated in a consistent manner with the PeleC reactive Navier-Stokes formulation. The Poisson equation for the electrostatic potential is solved in conjunction with the conservation of charged species. The solver implementation is validated against established benchmarks. The benchmarking exercise paves the way for future three-dimensional large-scale simulations of coupled low-temperature plasma-assisted ignition in turbulent reactive flows.

I. Nomenclature

 ρ = density

u = bulk gas velocity

p = pressure

 Π = diffusive transport flux for momentum

g = gravitational acceleration

U = Total energy

 $\dot{\omega}_k$ = production rate of species k

Q = diffusive transport flux for energy

 $v_{\rm eff}$ = effective velocity

 Y_k = mass fraction of species k

 \mathcal{F}_k = diffusive transport flux for species k

 z_k = charge number of species k

E = electric field

 μ_k = mobility of species k ϕ = electric potential

e = unit charge

 $\varepsilon_0 = \text{vacuum permittivity}$ $\rho_c = \text{space charge density}$

 S_{ph} = photoionization source term

 p_q = quenching pressure S_{ion} = ionization rate

 n_k = number density of species k

 k_B = Boltzmann constant T_e = electron temperature

 m_e = electron mass

E/N = reduced electric field

^{*}Graduate Research Assistant, Department of Aerospace Engineering, The University of Texas at Austin.

[†]Associate Professor, Department of Aerospace Engineering, The University of Texas at Austin.

[‡]Postdoctoral Researcher, The National Renewable Energy Laboratory.

[§]Researcher, The National Renewable Energy Laboratory.

[¶]Group Manager III, The National Renewable Energy Laboratory.

II. Introduction

Streamer discharges arise as self-supported ionization waves propagating from areas of high electric fields towards areas where the electric field is below breakdown. These waves are sustained by a large electric field at the tip of the streamer propagating through a gaseous or fluid medium. Streamers are precursors to the development of spark and arc discharges encountered in the field of plasma-assisted combustion (PAC). Streamers generated by nanosecond pulsed discharges (NSPD) have become an area of particular interest due to their relevance in PAC. NSPDs can enhance combustion under challenging conditions such as lean and dilute mixtures encountered in internal combustion engines and gas turbines [1–6], supersonic combustion [7, 8], and actuation in supersonic environments [9]. Combustion enhancement through the use of NSPDs includes kinetic enhancement, thermal heating, and the modification of transport properties.

NSPDs fall in the regime of low-temperature plasmas (LTP), where the electron temperature may far exceed the gas temperature, which is near ambient. In the context of plasma assisted combustion, NSPDs are typically applied between two pin electrodes, where the enhanced electric field near the pin tips leads to the development and propagation of a streamer. The streamer closes the gap and forms a conducting plasma channel that is characterized by an elevated electron temperature O(1-5 eV) and large electron populations $O(10^{18}-10^{23} \text{ m}^{-3})$. This channel is key to the deposition of energy through joule heating, the generation of electronically and vibrationally excited species, and production of combustion radicals. The resulting "fast" and "slow" heating processes [10, 11] associated with the relaxation of electronically and vibrationally excited species, and the generation of new kinetic pathways are key to supporting an ignition event.

Over the past few decades, efforts have been undertaken to better understand and model the broad problem of plasma-assisted combustion. Several experimental studies have focused on developing more accurate kinetic mechanisms describing the interactions of LTP with common hydrocarbon fuels [12–18]. The simulation of streamers in air has also been extensively studied in 2D [19–21], with some results in 3D as well [22–25]. Numerical studies of plasma-assisted ignition (PAI) in multiple dimensions exist [26, 27], but often rely on simplified kinetics mechanisms and modeling, and use of axisymmetric configurations, although streamers are known to undergo branching and other three-dimensional instabilities, especially at elevated pressures of interest to combustion applications.

The use of high-fidelity simulations to model the discharge and the subsequent relaxation period is key to the understanding the full ignition process. However, there are significant practical obstacles that must be overcome. The modeling of electrons and plasma processes results in very stiff dynamics over discharge and relaxation phases. The spatial resolution requirements at the streamer head are of the order of a few microns, very small compared to the length scales of interest O(10 mm). Finally, the complexity of a mechanism that captures the coupling between plasma and combustion kinetics results in a large number of species even after reduction [28]. The massively parallel, GPU-ready reactive Navier-Stokes solver PeleC [29, 30] provides a platform to address these challenges. PeleC is built on top of the AMReX adaptive mesh refinement library supported by the Department of Energy (DOE) Exascale Computing Project (ECP). PeleC provides AMR capabilities, detailed kinetics and thermochemistry models, embedded boundary geometry representation, and compatibility with low Mach solvers PeleLM/PeleLMeX. In this paper, a benchmarking exercise for the simulation of low-temperature plasma streamer discharges [31] is presented, paving the way towards future progress in the simulation of three-dimensional plasma assisted combustion simulations in turbulent flows.

III. Numerical Model

A. Governing equations

The reactive Navier-Stokes equations are extended to include a drift-diffusion closure, and joule heating. The temporal evolution of density, momentum, total energy density, and species mass fractions are modeled as

$$\frac{\partial \rho}{\partial t} = -\nabla \cdot (\rho \mathbf{u}), \tag{1}$$

$$\frac{\partial \rho \mathbf{u}}{\partial t} = -\nabla \cdot (\rho \mathbf{u} \mathbf{u} - p\mathbf{I} + \mathbf{\Pi}), \qquad (2)$$

$$\frac{\partial t}{\partial t} = -\nabla \cdot (\rho \mathbf{u} U + \rho \mathbf{u}) + \nabla \cdot \mathbf{Q} + e n_e \mu_e \mathbf{E} \cdot \mathbf{E},$$

$$\frac{\partial \rho Y_k}{\partial t} = -\nabla \cdot (\rho (\mathbf{u} + z_k \mu_k \mathbf{E}) Y_k) - \nabla \cdot \mathcal{F}_k + \rho \dot{\omega}_k.$$
(3)

$$\frac{\partial \rho Y_k}{\partial t} = -\nabla \cdot (\rho(\mathbf{u} + z_k \mu_k \mathbf{E}) Y_k) - \nabla \cdot \mathcal{F}_k + \rho \dot{\omega}_k. \tag{4}$$

Transport equations model the evolution of density ρ , momentum ρu , total energy density ρU , and individual species mass densities ρY_k . Diffusive fluxes for momentum, energy density, and species mass densities are Π , Q, and \mathcal{F}_k , while p and $\dot{\omega}_k$ represent pressure and production of species k. Transport coefficients (viscosity, diffusivity, and thermal conductivity) are calculated following the approximations by Ern and Giovangigli [32]. The velocity of the charged species is calculated as the sum of the bulk velocity u, and the drift velocity $z_k \mu_k E$ due to the influence of the electric field, where z_k and μ_k are the charge number and mobility of species k, and E is the electric field. The electric field is obtained solving the Poisson problem for the electrostatic potential ϕ

$$\Delta \phi = -\frac{1}{\varepsilon_0} \rho_c,\tag{5}$$

where the charge density is $\rho_c = e \sum_k z_k n_k$, and ε_0 is the vacuum permittivity. Electron properties, such as the mobility μ_e , diffusivity \mathcal{D}_e , temperature T_e , and various rate coefficients are evaluated as functions of the reduced electric field E/N, according to the local field approximation (LFA) [33].

The joule heating term is calculated using the unit charge e, the electron number density and mobility n_e and μ_e , and electric field E. This assumption neglects the effect of other charged species due to the much smaller mobility of ions. Consistent with the LFA, the mean electron energy is a function of the local reduced electric field, and is not modeled separately from the gas energy, as in a local mean energy approximation (LMEA) [34]. It follows that energy gained by the electrons through joule heating effects during the pulse increases the gas energy density instantaneously, which is an approximation. As this study is concerned with time scales relevant to streamer propagation with no significant joule heating, it is assumed that the error incurred by assuming instantaneous energy deposition is negligible.

B. Numerical methods

To resolve sharp gradients encountered at the streamer head, grid spacing $O(1 \mu m)$ is required. As these gradients are limited to a very small region of the overall domain, the finite volume adaptive mesh refinement (AMR) library AMReX [29] is used to increase grid resolution only where needed. A coarse mesh is defined on the entire domain, and a hierarchy of successively finer grids resolve steep gradients in the solution, with up to 6 additional levels of refinement (with a refinement factor of 2 in the side of the cubic control volumes between levels). The refinement criteria may be defined on any state or derived variable, gradient of a state or derived variable, or spatial location. This includes but is not limited to temperature, pressure, temperature and pressure gradients, number density, number density gradient, electric field and electric field gradient.

For propagating streamers, we found that a robust refinement criteria is defined based on the gradient of the reduced electric field E/N (or electric field). Cells are tagged for refinement at a given level when the absolute value of the finite difference between adjacent cells exceeds a user-specified threshold. The specific values for each case will be discussed for each benchmark case. These parameters ensure that the streamer head is resolved appropriately, while additional resolution is not wasted in regions where it is not necessary.

Due to their small mass relative to ions, time step size constraints are largely driven by electron dynamics. Specifically, the electron drift and diffusion Courant-Friedrichs-Lewy (CFL) condition and dielectric relaxation time scale (which is associated with the coupling between changes in space charge density and electric field) control the time step size δt that ensures numerical stability of the solution. Following [35], δt is calculated as

$$\delta t = \min(C_A \, \delta t_A, C_E \, \delta t_E, C_D \delta t_D), \tag{6}$$

$$\delta t_A = \min\left(\frac{\Delta x}{|\mathbf{v}|_{\text{eff},e}}\right),\tag{7}$$

$$\delta t_E = \min\left(\frac{\varepsilon_0}{e\mu_e n_e}\right),\tag{8}$$

$$\delta t_D = \min\left(\frac{\Delta x^2}{6\mathcal{D}_e}\right),\tag{9}$$

where δt_A , δt_D , and δt_E represent the electron drift, electron diffusion, dielectric relaxation time scale constraints, and minimization occurs across the entire domain and all AMR levels. That is, we are advancing all levels in the AMR hierarchy with the same time step size. The coefficients C_A , C_E , and C_D depend on the numerical method used for time integration. The coefficient C_A is always 0.3 due to the restriction of the Method-of-lines (MOL) advancement strategy. C_E is either set to 0.5 for explicit time integration of the electric field, or 10.0 if we employ a semi-implicit time-integration of the Poisson equation [36]. C_D is set to 0.3 if we use an explicit time-integration of the electron diffusion term, or neglected (set to infinity) if we use an implicit method. In this study, the combination of the semi-implicit approximation to the electric field and explicit diffusion was used to produce the results. Thanks to the fully-implicit time-integration of chemistry, chemical time scales do not impose any time step restriction.

Advection of the conserved variables (U) is discretized using a Godunov scheme with characteristic extrapolation to cell faces and a Riemann solver. Diffusive sources are discretized using a second-order centered approach, and transport coefficients based on the approximations by Ern and Giovangigli [32]. Time advancement uses a predictor-corrector approach, whereby the advective and diffusive sources S_{AD} are calculated multiple times within each step to construct approximations to the conserved variable U^{**}

$$S_{AD}^{n} = A(U^{n}) + D(U^{n})$$

$$\tag{10}$$

$$U^* = U^n + \Delta t (S_{AD}^n + \omega_r) \tag{11}$$

$$S_{AD}^{n+1} = A(U^*) + D(U^*)$$
(12)

$$U^{**} = \frac{1}{2}(U^n + U^*) + \frac{\Delta t}{2}(S_{AD}^{n+1} + \omega_r), \tag{13}$$

where A and D represent the advective and diffusive operators, while ω_r is a time-lagged reactive source. From here, an advective/diffusive forcing term is calculated

$$F_{AD} = \frac{1}{\Lambda t} (U^{**} - u^n) - \omega_r, \tag{14}$$

after which the solution at the next time step is obtained by integrating U^n with F_{AD} and the reactive sources until time n+1 using CVODE [37]. The time-lagged reactive source term is then updated for the next time step

$$\omega_r = \frac{U^{n+1} - U^n}{\Lambda t} - F_{AD}. \tag{15}$$

The time advancement strategy is summarized in algorithm 1. It is again emphasized that the diffusion of electrons can be handled implicitly to relax the stability constraint.

IV. Results

A. Bagheri Benchmark

The streamer code benchmark outlined in [31] is used to validate the simulation of low-temperature plasma streamer discharges implemented in PeleC. The overview of the benchmark case is briefly presented below, but the reader is referred to the original article [31] for implementation details, and a full description of the various solvers employed. The general geometry is the same across all cases, consisting of an axisymmetric domain of $1.25 \times 1.25 \text{ cm}^2$. For our purposes, this is generalized to a rectangular domain of $2.5 \text{ cm} \times 1.25 \text{ cm} \times 2.5 \text{ cm}$. In the original benchmark, only electrons e and one species of positive ions p is considered, and the transport of positive ions is neglected so that the

Algorithm 1 PeleC advancement framework

```
1: procedure Advance(U(\rho, \rho u, U, n_k))
 2:
             while t < t_{\text{out}} do
                   \mathbf{E}^{n+1} = -\nabla \phi^{n+1}
 3:
                                                                                           \triangleright Applied voltage \phi_{app} at anode, explicit or semi-implicit approx.
                   \begin{split} S_{ph} &= S_{ph}(\boldsymbol{U}^n) \\ \boldsymbol{S}^* &= AD(\boldsymbol{U}^n, \boldsymbol{E}^{n+1}) \end{split}
                                                                                                                             ▶ Calculated using 3-term Helmholtz approx.
 4:
 5:
                                                                                                                    > Advective/diffusive sources and boundary fluxes
                       D_{Y_E} = D(Y_E^n)

S_U^* + = S_{jh}(U^n, E^{n+1})
                                                                                                    \triangleright Implicit evaluation of the Y_E diffusive source if necessary
 6:
 7:

    Joule heating increases gas energy

                   U^* = U^n + \Delta t (S^* + \omega_r)
 8:
                   \mathbf{S}^{n+1} = AD(\mathbf{U}^*, \mathbf{E}^{n+1})
 9.
                       \begin{split} D_{Y_E} &= D(Y_E^*) \\ S_U^{n+1} + &= S_{jh}(\pmb{U}^*, \pmb{E}^{n+1}) \end{split}
10:
11:
                   U^{**} = \frac{1}{2}(U^n + U^*) + \frac{\Delta t}{2}(S^{n+1} + \omega_r)
12:
                   \mathbf{F}_{AD} = \frac{1}{\Delta t} (\mathbf{U}^{**} - \mathbf{U}^n) - \omega_r
13:
                                                                                                                                                ▶ Advective/diffusive forcing term
                   \omega_r = \omega_r(U^n, F_{AD}, S_{ph})
U^{n+1} = U^n + \Delta t(F_{AD} + \omega_r)
                                                                                                                                                            ▶ Integrated using CVODE
14:
15:
             end while
16:
17: end procedure
```

governing equations are

$$\Delta \phi = -\frac{e(n_p - n_e)}{\epsilon_0},\tag{16}$$

$$\frac{\partial n_e}{\partial t} + \nabla \cdot (-n_e \mu_e E - \mathcal{D}_e \nabla n_e) = \bar{\alpha} \mu_e ||E|| n_e + S_{\text{ph}},$$

$$\frac{\partial n_p}{\partial t} = \bar{\alpha} \mu_e ||E|| n_e + S_{\text{ph}},$$
(17)

$$\frac{\partial n_p}{\partial t} = \bar{\alpha} \mu_e ||E|| n_e + S_{\text{ph}},\tag{18}$$

where $\bar{\alpha}$ is the effective ionization coefficient, and $S_{\rm ph}$ is the photoionization source term. It is noted that the current solver was developed for fully coupled streamer simulations with the reactive multi-component Navier-Stokes equations. As such, the simplification of the full model can be error prone, and was deemed not necessary for the validation exercise. Instead, the multi-component is still considered along with the computation of all advective and diffusive fluxes of all state variables, but the majority of the terms are zeroed before the advancement of the solution such that the only nonzero terms remaining are the advection and diffusion of electrons, and the chemical source term of electrons and positive ions as described in the governing equations. This procedure has consequences when assessing the performance of the code. For the expressions of the effective ionization coefficient $\bar{\alpha}$, mobility μ_e , electron diffusion coefficient \mathcal{D}_e , and photoionization $S_{\rm ph}$ the reader is referred to the original publication [31].

The gas properties are also the same across all cases, with dry air at p = 1 bar and T = 300 K. A homogeneous background electric field of 15 kV/cm (pointing downwards) is applied, which is well below breakdown. A Gaussian profile of positive charge is initialized in the gap to enhance the local electric field due to space charge and cause the formation of a positive streamer that propagates towards the cathode

$$n_p(x, y, z) = n_0 \exp\left[-\frac{x^2 + (y - y_0)^2 + z^2}{\sigma^2}\right].$$
 (19)

The field n_p is added to a background ionization n_i to both electrons and positive ions. For all cases $n_0 = 5.0 \times 10^{-18}$ m^{-3} , $y_0 = 1.0$ cm, and $\sigma = 0.4$ mm. The resulting profile of the electric field at the onset of the simulation is shown in

For all cases, the refinement criterion is as follows: a coarse base mesh of $128 \times 64 \times 128$ cells is initialized with a resolution of $\Delta x = 0.2$ mm, a constant refinement criterion of 2 is used for up to 6 additional levels of refinement resulting in a maximum resolution of 3 μ m. The refinement criterion is based on the reduced electric field gradient. For every cell, if the reduced electric field difference across any two adjacent cells is greater than 10 Td, then the cell is tagged for refinement. If the reduced electric field value exceeds 120 Td, the cell is tagged for refinement to level 3 corresponding to a resolution $24 \mu m$. This strategy was found to be adequate for all cases tested in this work. The

Table 1 Summary of test cases established in the streamer discharge benchmark [31]

Case	Background ionization	Photoionization
Case 1	10^{13} m^{-3}	No
Case 2	10^9 m^{-3}	No
Case 3	10^9 m^{-3}	Yes

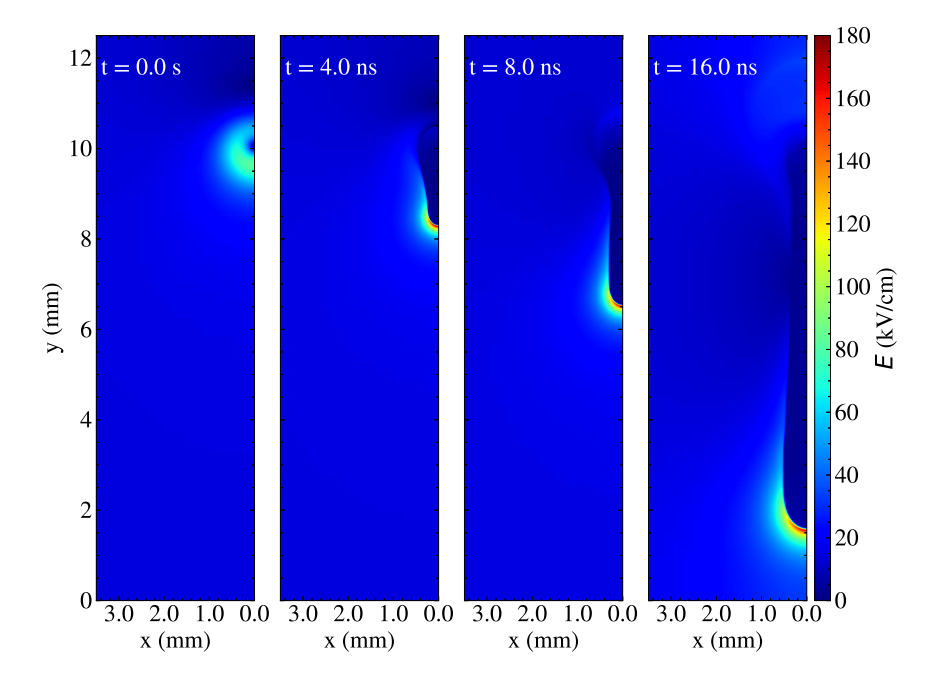


Fig. 1 Magnitude of the electric field at various instants in time, illustrating the downward propagation of the streamer in Case 1.

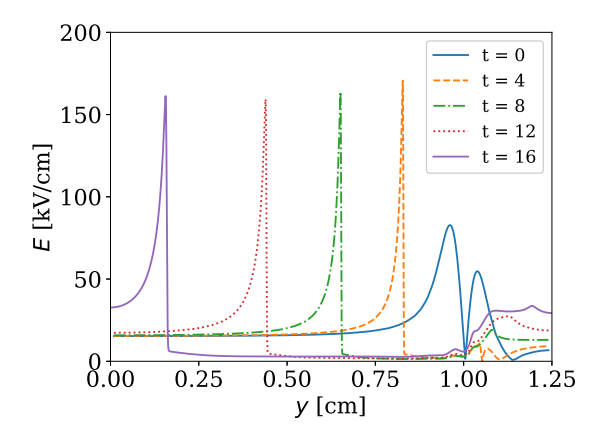
differences in the three cases are limited to different background ionization levels and inclusion of photoionization, as summarized in Table 1.

1. Case 1

The first case is the one considered to be least challenging for plasma solvers. It has a relatively high background ionization $n_i = 10^{-13} \text{ m}^{-3}$ and photoionization is neglected. The relatively high background ionization lowers spatial gradients in the number densities of positive ions and electrons, and also results in lowering the electric field at the tip of the streamer. While photoionization has a similar smoothing effect, it comes with significant cost and complexity to solvers. These simplifications make the overall simulation more affordable from a computational perspective.

The overall discharge evolution is shown in Fig. 1, where the magnitude of the electric field is reported at several instants in time. The kernel of positive charge enhances the electric field above breakdown and leads to the formation of a positive streamer. The magnitude of the electric field at the tip of the streamer increases steadily until around 4 ns, when it achieves a quasi-steady value for the rest of the streamer propagation. The streamer continues to propagate downwards, leaving a plasma channel in its wake until 16 ns, when the streamer has almost completely traversed the domain.

The magnitude of the electric field and number density of electrons are shown in Fig. 2, adhering to the format provided in the original reference [31] to ease visual comparisons. The axial profiles build upon the results provided in the previous figure, illustrating sharp gradients encountered in both the electric field and number density of electrons. As the streamer propagates downwards, an ionized path with large populations of electrons is left in its wake along with a near-zero electric field that is much lower than the constant electric field imposed across the gap. The similarity of the



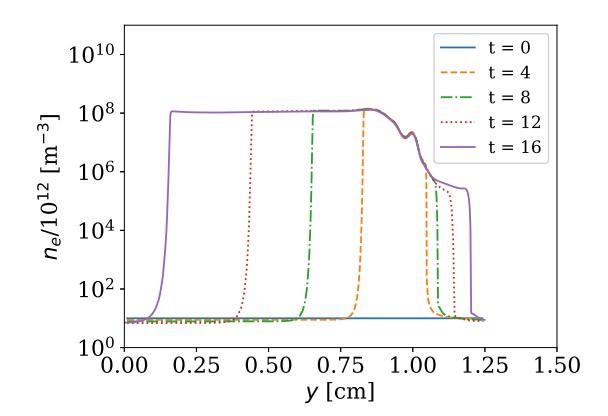


Fig. 2 Axial profiles of the magnitude of the electric field and number density of electrons in the center of the gap illustrating the downward propagation of the streamer. The time in nanoseconds is provided in the legend.

profiles and slices of the solution indicate good qualitative agreement between the results generated by our solver and those provided in the original streamer benchmark [31].

The overall agreement of results shown here compared to those reported in the streamer benchmark study is very good, however a comparison through visual inspection is of limited value. Below, we present a quantitative comparison between results from our solver and other established streamer solvers through metrics that take into account streamer velocity, degree of ionization, and charge conservation. The comparisons are made for each solver's "standard resolution" as defined in the original reference, where most solvers match closely the minimum spatial resolution of 3 μ m used in our study. In Fig. 3 we show the streamer length L(t) and adjusted streamer length L(t) - vt for solutions from the various solvers. Our results are very close to those from both the "CWI" [25] and "DE" [38] solvers (less than 0.25 mm difference), and effectively identical to "CWI".

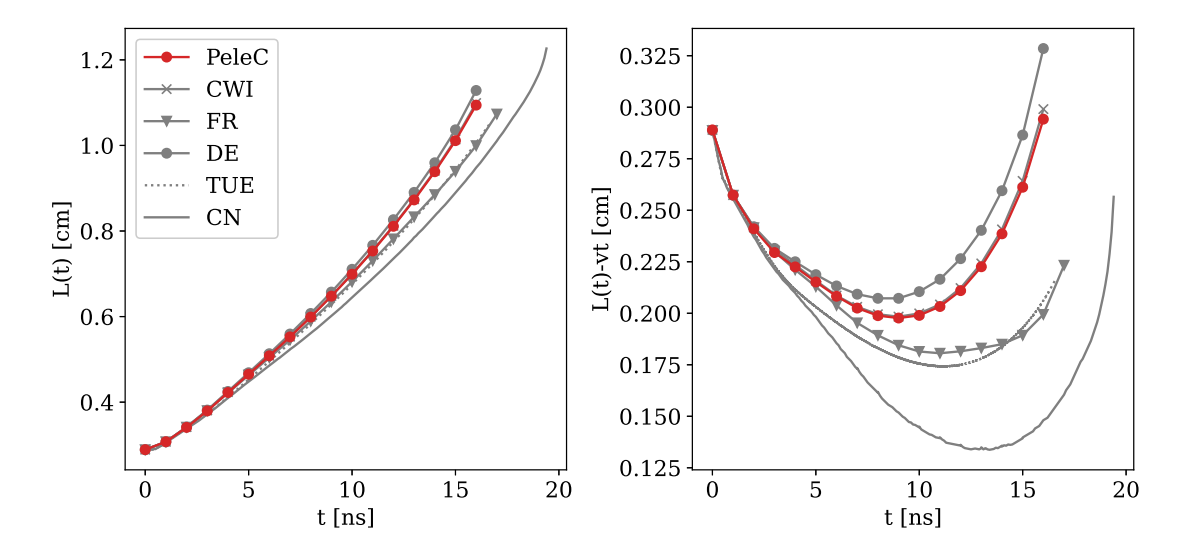


Fig. 3 Case 1: Comparison of streamer length L(t), defined as 1.25 cm - y_{max} , where y_{max} is the location of the maximum electric field at time t, and adjusted streamer length L(t) - vt (where v = 0.05 cm/ns) for the various solvers. Labels given to the solvers are the same as in the original reference [31].

Further quantitative comparisons are shown in Fig. 4, where the maximum electric field $E_{\rm max}$ and total charge Q are shown as a function of the streamer length L(t). The total charge Q is defined as the volume integral of the space charge density over the entire computational domain. In terms of the maximum electric field, again we observe a value that is very close to the baseline established by the "DE" and "CWI" solvers (less than 5 kV/cm difference), although slightly larger throughout most of the streamer propagation phase. Our solver also performs very well in terms of charge conservation as observed in the results of total charge Q as a function of the streamer length. As a finite volume (FV) solver, it is in agreement with other FV solvers from the original reference.

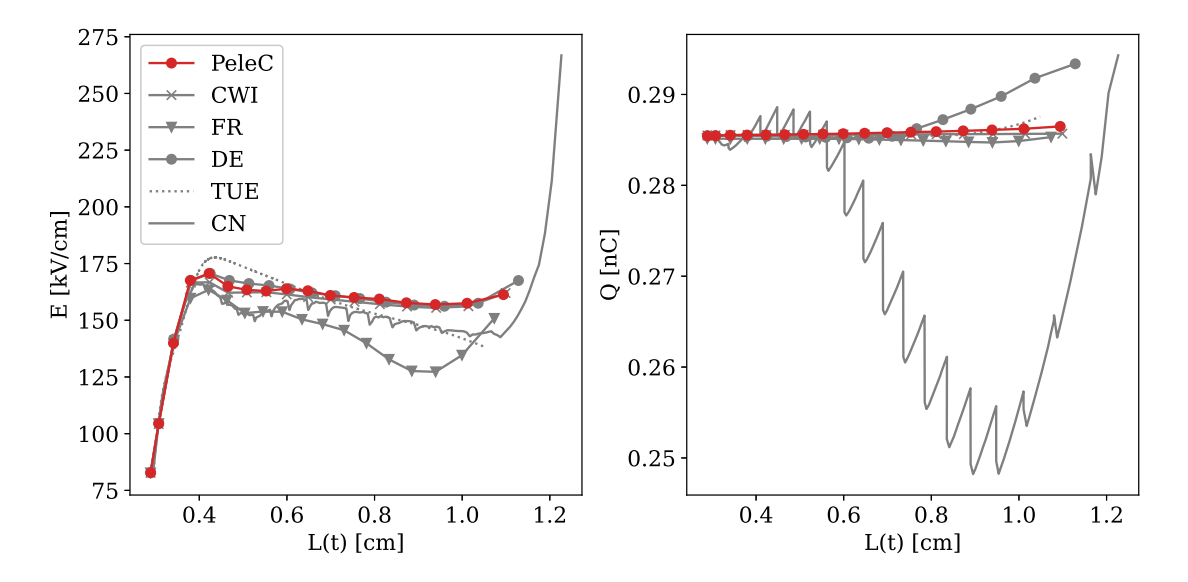


Fig. 4 Case 1: Comparison of maximum electric field $E_{\rm max}$ and total charge Q as a function of the streamer length L(t) across results for all streamer solvers.

2. Case 2

The second test case is designed to be more challenging, starting from a significantly lower background ionization of 10⁹ m⁻³. This level of ionization causes sharper gradients, which in turn induce a larger electric field at the tip of the streamer compared to Case 1. These aspects make the second benchmark more challenging from a computational perspective. The configuration remains unchanged and is qualitatively very similar, therefore, we limit our discussion to quantitative comparisons across solvers. The same metrics are used to compare across results.

The streamer length L(t) and adjusted streamer length L(t) - vt for Case 2 are shown in Fig. 5. As previously mentioned, this case implies steeper gradients and as such, differences between the results produced by the solvers are exacerbated. The solution computed by our solver lies between the solution produced by the "DE" and "FR" codes. From the original reference [31], this benchmark required increased resolution and finer grids for almost all solvers. The standard resolution results in some numerical instabilities for the solvers relying on an explicit approximation to the electric field, and for this reason solution with the highest spatial resolution reported (0.8 μ m) from the "CWI" solver is also included in the plots.

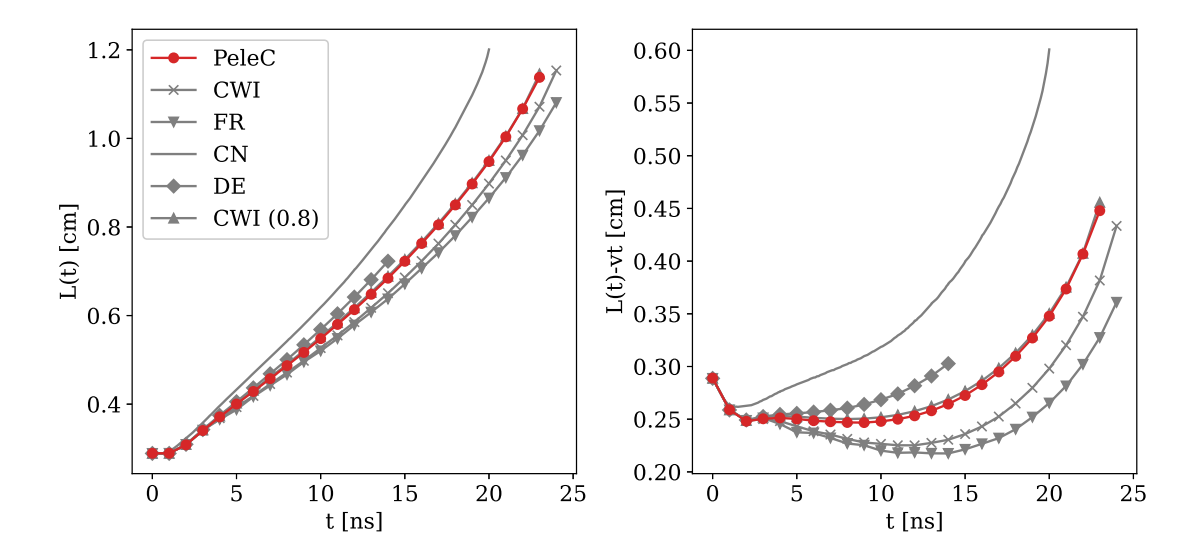


Fig. 5 Case 2: Comparison of streamer length L(t), defined as 1.25 cm - y_{max} , where y_{max} is the location of the maximum electric field at time t, and adjusted streamer length L(t) - vt (where v = 0.03 cm/ns) across the different streamer codes. Labels given to the solvers are the same as in the original reference [31].

The maximum electric field E and total charge Q in the domain is shown in Fig. 6. It is again observed that the spread of the different solver results is larger than that encountered in the previous case. The difference between the largest (DE) and the smallest (CN) values for the maximum electric field is of over 90 kV/cm at certain instant during the propagation compared to about 40 kV/cm in the previous case. Our computed value is in between those computed by the "DE" solver and the "CWI,FR" solvers, although "FR" is using twice the resolution compared to the others. At around 20 ns, the solution in PeleC appears to run into numerical difficulties as indicated by the fluctuations in the maximum electric field and an apparent minor loss of charge.

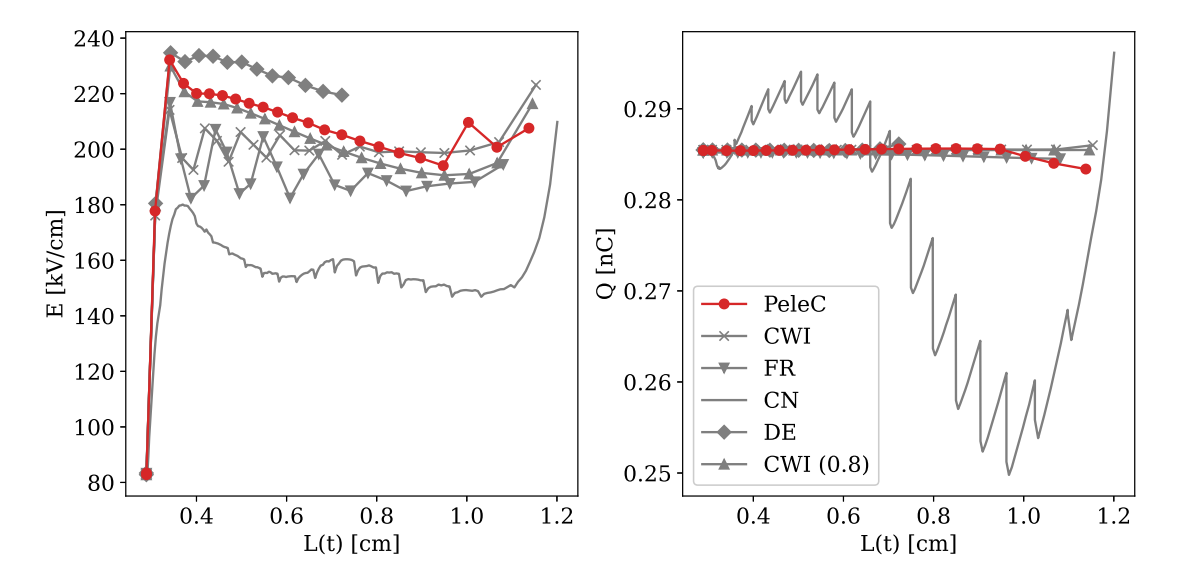


Fig. 6 Case 2: Comparison of maximum electric field E_{max} and total charge Q as a function of streamer length L(t) across results for all streamer solvers.

3. Case 3

The third case is identical to Case 2, except that photoionization is included. Photoionization smoothens large gradients encountered in Case 2, resulting in a less demanding simulation. Our solver approximates photoionization by solving three sequential Helmholtz equations as explained in Bourdon et al. [39]. Including photoionization according to this model can add a significant computational cost (approximately 20-25%).

Solutions are compared with regard to the same set of metrics used for the previous two cases. Results on the streamer length L(t) and adjusted streamer length L(t) - vt are compared across the different solvers in Fig. 7, and as in the original reference [31], fewer solvers are included in this test. There is remarkable agreement by all the solvers, to a degree that was not observed in previous cases. Calculated streamer lengths are within 0.5 mm of each other, with the exception of the results from the "CN" solver. This seems to imply that the gradients encountered in this case are smoother than those encountered with a background ionization of $n_i = 1 \times 10^{13} \text{ m}^{-3}$.

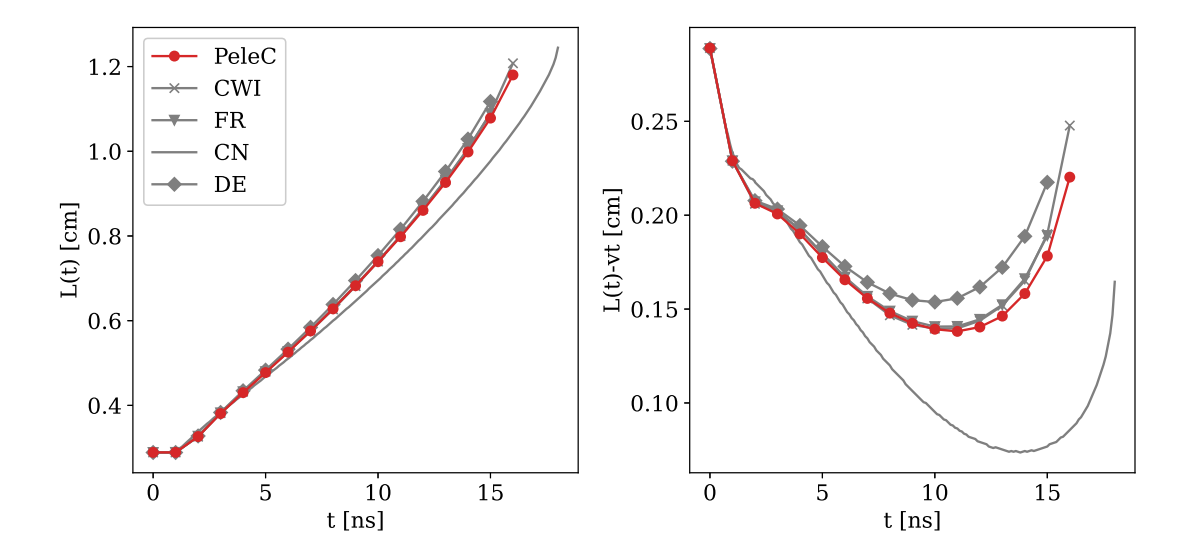


Fig. 7 Case 3: Comparison of streamer length L(t), defined as 1.25 cm - y_{max} , where y_{max} is the location of the maximum electric field at time t, and adjusted streamer length L(t) - vt (where v = 0.06 cm/ns) across the different streamer codes. Labels given to the solvers are the same as in the original reference [31].

Similar conclusions are made based on data shown in Fig. 8. Again, remarkable agreement is found across results from the various solvers in terms of the maximum electric field, where the difference is limited to about 5 kV/cm ("CN" again being the exception). Our solver performs well in terms of charge conservation, with similar performance to that observed in Case 1.

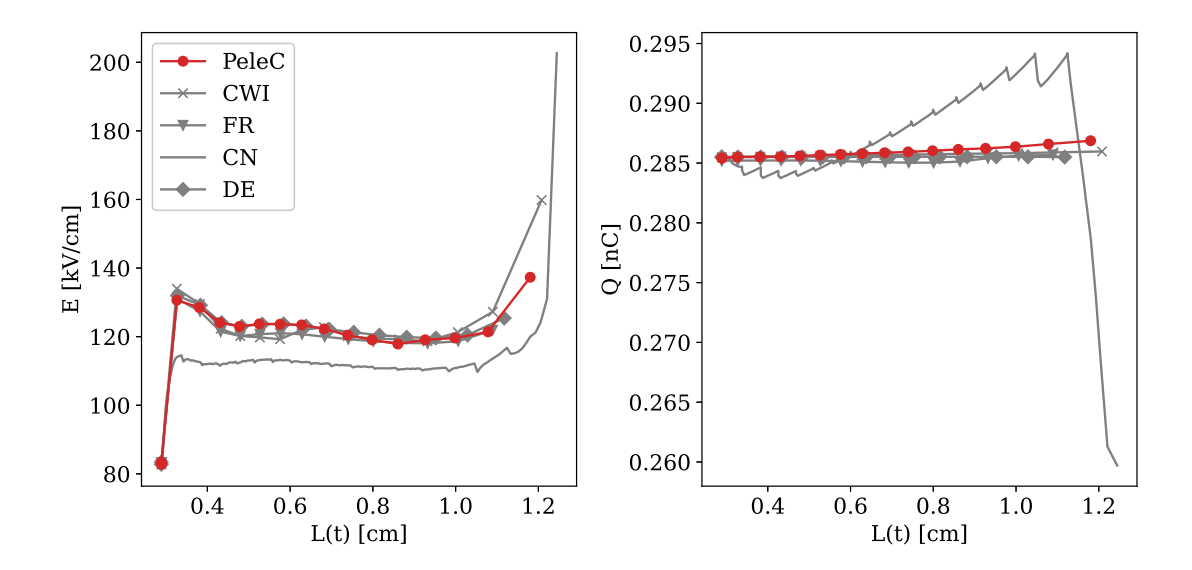


Fig. 8 Case 3: Comparison of maximum electric field E_{max} and total charge Q as a function of streamer length L(t) for all results produced by the various solvers.

V. Conclusions

In this study, we benchmark the performance of a coupled low-temperature reactive Navier-Stokes solver against a well-known set of test cases for plasma streamer discharges. The solver is based on the reactive Navier-Stokes solver PeleC built on the adaptive mesh refinement library AMReX. The drift-diffusion fluid model for low-temperature discharges is coupled with the reactive Navier-Stokes with explicit calculation of advective and diffusive terms, and a semi-implicit scheme to advance the electrostatic potential. The adaptive mesh refinement strategy targets values and gradients of the reduced electric field.

The benchmark established by Bagheri et al. [31] is used to compare the current solver against other low-temperature plasma discharge solvers. The benchmark consists of three cases at 300 K and 1 bar where prescribed values are specified for transport coefficients and ionization rates. The cases differ in their background ionization density and for the inclusion of photoionization. The lower background ionization density case in particular induces large gradients that are challenging for solvers. Quantitative metrics are considered including streamer location, maximum electric field, and conservation of charge. Excellent agreement is observed for all cases, especially with the solvers discussed in [25] ("CWI") and [38] ("DE"). Some numerical difficulties are encountered at the late stages of Case 2, where the gradients in the number density of charges are steep and the most challenging.

The successful completion of this benchmark study establishes confidence in the implementation of the solver. The solver has demonstrated performance results in some of the most powerful computers in the world and is compatible with the Low-Mach solvers suite PeleLM/PeleLMeX. The current work paves the way for ignition simulations of plasma assisted ignition using Nanosecond Repetitively Pulsed discharges in three-dimensional configurations featuring turbulent flows.

Acknowledgments

This research was supported by DOE contract DE-EE0008874 and NSF grant # 1903775, along with computation resources provided by the Texas Advanced Computing Center (TACC) and National Renewable Energy Laboratory (NREL).

References

[1] Serbin, S., Mostipanenko, A., Matveev, I., and Topina, A., "Improvement of the gas turbine plasma assisted combustor characteristics," 49th AIAA aerospace sciences meeting including the new horizons forum and aerospace exposition, 2011, p. 61.

- [2] Santner, J., Dryer, F. L., and Ju, Y., "The effects of water dilution on hydrogen, syngas, and ethylene flames at elevated pressure," *Proceedings of the Combustion Institute*, Vol. 34, No. 1, 2013, pp. 719–726.
- [3] Moeck, J., Lacoste, D., Laux, C., and Paschereit, C., "Control of combustion dynamics in a swirl-stabilized combustor with nanosecond repetitively pulsed discharges," 51st AIAA Aerospace Sciences Meeting including the New Horizons Forum and Aerospace Exposition, 2013, p. 565.
- [4] Sevik, J., Wallner, T., Pamminger, M., Scarcelli, R., Singleton, D., and Sanders, J., "Extending lean and exhaust gas recirculation-dilute operating limits of a modern gasoline direct-injection engine using a low-energy transient plasma ignition system," *J. Eng. Gas Turbine Power*, Vol. 138, No. 11, 2016.
- [5] Shiraishi, T., Urushihara, T., and Gundersen, M., "A trial of ignition innovation of gasoline engine by nanosecond pulsed low temperature plasma ignition," *J. Phys. D: Appl. Phys.*, Vol. 42, No. 13, 2009, p. 135208.
- [6] Khacef, A., Cormier, J. M., and Pouvesle, J. M., "NOx remediation in oxygen-rich exhaust gas using atmospheric pressure non-thermal plasma generated by a pulsed nanosecond dielectric barrier discharge," J. Phys. D: Appl. Phys., Vol. 35, No. 13, 2002, p. 1491.
- [7] Leonov, S. B., and Yarantsev, D. A., "Plasma-induced ignition and plasma-assisted combustion in high-speed flow," *Plasma Sources Sci. Technol.*, Vol. 16, No. 1, 2006, p. 132.
- [8] Lefkowitz, J. K., and Ombrello, T., "Reduction of flame development time in nanosecond pulsed high frequency discharge ignition of flowing mixtures," *Combust. Flame*, Vol. 193, 2018, pp. 471–480.
- [9] Starikovskii, A. Y., Nikipelov, A., Nudnova, M., and Roupassov, D., "SDBD plasma actuator with nanosecond pulse-periodic discharge," *Plasma Sources Sci. Technol.*, Vol. 18, No. 3, 2009, p. 034015.
- [10] Popov, N., "Fast gas heating in a nitrogen–oxygen discharge plasma: I. Kinetic mechanism," J. Phys. D: Appl. Phys., Vol. 44, No. 28, 2011, p. 285201.
- [11] Lanier, S., Shkurenkov, I., Adamovich, I. V., and Lempert, W. R., "Two-stage energy thermalization mechanism in nanosecond pulse discharges in air and hydrogen–air mixtures," *Plasma Sources Science and Technology*, Vol. 24, No. 2, 2015, p. 025005.
- [12] Togai, K., Tsolas, N., and Yetter, R. A., "Kinetic modeling and sensitivity analysis of plasma-assisted oxidation in a H2/O2/Ar mixture," Combust. Flame, Vol. 164, 2016, pp. 239–249.
- [13] Winters, C., Eckert, Z., Yin, Z., Frederickson, K., and Adamovich, I., "Measurements and kinetic modeling of atomic species in fuel-oxidizer mixtures excited by a repetitive nanosecond pulse discharge," J. Phys. D: Appl. Phys., Vol. 51, No. 1, 2017, p. 015202.
- [14] Winters, C., Hung, Y.-C., Jans, E., Eckert, Z., Frederickson, K., Adamovich, I. V., and Popov, N., "OH radical kinetics in hydrogen-air mixtures at the conditions of strong vibrational nonequilibrium," *J. Phys. D: Appl. Phys.*, Vol. 50, No. 50, 2017, p. 505203.
- [15] Eckert, Z. S., "Energy Transfer in Non-Equilibrium Reacting Gas Flows: Applications in Plasma Assisted Combustion and Chemical Gas Lasers," Ph.D. thesis, The Ohio State University, 2018.
- [16] Yang, S., Gao, X., Yang, V., Sun, W., Nagaraja, S., Lefkowitz, J. K., and Ju, Y., "Nanosecond pulsed plasma activated C2H4/O2/Ar mixtures in a flow reactor," J. Propul. Power, 2016, pp. 1240–1252.
- [17] Lefkowitz, J. K., Guo, P., Rousso, A., and Ju, Y., "Species and temperature measurements of methane oxidation in a nanosecond repetitively pulsed discharge," Vol. 373, No. 2048, 2015, p. 20140333.
- [18] Rousso, A., Mao, X., Chen, Q., and Ju, Y., "Kinetic studies and mechanism development of plasma assisted pentane combustion," *Proc. Combust. Inst.*, Vol. 37, No. 4, 2019, pp. 5595–5603.
- [19] Pancheshnyi, S., and Starikovskii, A. Y., "Two-dimensional numerical modelling of the cathode-directed streamer development in a long gap at high voltage," *J. Phys. D: Appl. Phys.*, Vol. 36, No. 21, 2003, p. 2683.
- [20] Tholin, F., and Bourdon, A., "Influence of temperature on the glow regime of a discharge in air at atmospheric pressure between two point electrodes," *J. Phys. D: Appl. Phys.*, Vol. 44, No. 38, 2011, p. 385203.
- [21] Zakari, M., Caquineau, H., Hotmar, P., and Ségur, P., "An axisymmetric unstructured finite volume method applied to the numerical modeling of an atmospheric pressure gas discharge," J. Comput. Phys., Vol. 281, 2015, pp. 473–492.

- [22] Marskar, R., "An adaptive Cartesian embedded boundary approach for fluid simulations of two-and three-dimensional low temperature plasma filaments in complex geometries," J. Comput. Phys., Vol. 388, 2019, pp. 624–654.
- [23] Marskar, R., "3D fluid modeling of positive streamer discharges in air with stochastic photoionization," *Plasma Sources Sci. Technol.*, Vol. 29, No. 5, 2020, p. 055007.
- [24] Plewa, J., Eichwald, O., Ducasse, O., Dessante, P., Jacobs, C., Renon, N., and Yousfi, M., "3D streamers simulation in a pin to plane configuration using massively parallel computing," *J. Phys. D: Appl. Phys.*, Vol. 51, No. 9, 2018, p. 095206.
- [25] Teunissen, J., and Ebert, U., "Simulating streamer discharges in 3D with the parallel adaptive Afivo framework," J. Phys. D: Appl. Phys., Vol. 50, No. 47, 2017, p. 474001.
- [26] Kobayashi, S., Bonaventura, Z., Tholin, F., Popov, N. A., and Bourdon, A., "Study of nanosecond discharges in H2–air mixtures at atmospheric pressure for plasma assisted combustion applications," *Plasma Sources Sci. Technol.*, Vol. 26, No. 7, 2017, p. 075004.
- [27] Sharma, A., Subramaniam, V., Solmaz, E., and Raja, L. L., "Fully coupled modeling of nanosecond pulsed plasma assisted combustion ignition," J. Phys. D: Appl. Phys., Vol. 52, No. 9, 2018, p. 095204.
- [28] Bellemans, A., Kincaid, N., Deak, N., Pepiot, P., and Bisetti, F., "P-DRGEP: a novel methodology for the reduction of kinetics mechanisms for plasma-assisted combustion applications," *Proceedings of the Combustion Institute*, Vol. 38, No. 4, 2021, pp. 6631–6639.
- [29] Sitaraman, H., Yellapantula, S., de Frahan, M. T. H., Perry, B., Rood, J., Grout, R., and Day, M., "Adaptive mesh based combustion simulations of direct fuel injection effects in a supersonic cavity flame-holder," *Combust. Flame*, Vol. 232, 2021, p. 111531.
- [30] Henry de Frahan, M. T., Rood, J. S., Day, M. S., Sitaraman, H., Yellapantula, S., Perry, B. A., Grout, R. W., Almgren, A., Zhang, W., Bell, J. B., and Chen, J. H., "PeleC: An adaptive mesh refinement solver for compressible reacting flows," *The International Journal of High Performance Computing Applications*, Vol. 0, No. 0, 2022, p. 10943420221121151.
- [31] Bagheri, B., Teunissen, J., Ebert, U., Becker, M. M., Chen, S., Ducasse, O., Eichwald, O., Loffhagen, D., Luque, A., Mihailova, D., Plewa, J. M., van Dijk, J., and Yousfi, M., "Comparison of six simulation codes for positive streamers in air," *Plasma Sources Science and Technology*, Vol. 27, No. 9, 2018, p. 095002.
- [32] Ern, A., and Giovangigli, V., Multicomponent transport algorithms, Vol. 24, Springer Science & Business Media, 1994.
- [33] Ward, A., "Calculations of cathode-fall characteristics," J. Appl. Phys., Vol. 33, No. 9, 1962, pp. 2789–2794.
- [34] Park, S.-K., and Economou, D. J., "Analysis of low pressure rf glow discharges using a continuum model," J. Appl. Phys., Vol. 68, No. 8, 1990, pp. 3904–3915.
- [35] Vitello, P., Penetrante, B., and Bardsley, J., "Simulation of negative-streamer dynamics in nitrogen," *Phys. Rev. E*, Vol. 49, No. 6, 1994, p. 5574.
- [36] Ventzek, P. L., Sommerer, T. J., Hoekstra, R. J., and Kushner, M. J., "Two-dimensional hybrid model of inductively coupled plasma sources for etching," *Appl. Phys.*, Vol. 63, No. 5, 1993, pp. 605–607.
- [37] Hindmarsh, A. C., Brown, P. N., Grant, K. E., Lee, S. L., Serban, R., Shumaker, D. E., and Woodward, C. S., "SUNDIALS: Suite of nonlinear and differential/algebraic equation solvers," ACM Trans. Math. Software, Vol. 31, No. 3, 2005, pp. 363–396.
- [38] Becker, M. M., KÃ\(\times\)hlert, H., Sun, A., Bonitz, M., and Loffhagen, D., "Advanced fluid modeling and PIC/MCC simulations of low-pressure ccrf discharges," *Plasma Sources Science and Technology*, Vol. 26, No. 4, 2017, p. 044001.
- [39] Bourdon, A., Pasko, V., Liu, N., Célestin, S., Ségur, P., and Marode, E., "Efficient models for photoionization produced by non-thermal gas discharges in air based on radiative transfer and the Helmholtz equations," *Plasma Sources Sci. Technol.*, Vol. 16, No. 3, 2007, p. 656.